

# Body temperature enhanced adhesive, antibacterial and recyclable ionic hydrogel for epidermal electrophysiological monitoring

*Ying Liu<sup>#</sup>, Chan Wang<sup>#</sup>, Jiangtao Xue<sup>#</sup>, Guanhua Huang, Shuang Zheng, Ke Zhao, Jing Huang, Yiqian Wang, Yan Zhang, Tailang Yin<sup>\*</sup>, Zhou Li<sup>\*</sup>*

Y. Liu, C. Wang, X.J. Tao, J. Huang, Y. Q. Wang, Prof. Z. Li

CAS Center for Excellence in Nanoscience Beijing Key Laboratory of Micro-nano Energy and Sensor, Beijing Institute of Nanoenergy and Nanosystems, Chinese Academy of Sciences, Beijing 101400, China.

Y. Liu, C. Wang, Prof. Z. Li

School of Nanoscience and Technology, University of Chinese Academy of Sciences, Beijing 100049, China.

J. T. Xue

School of Life Science, Beijing Institute of Technology, Beijing 100081, China

G. H. Huang, S. Zheng, Prof. K. Zhao

State Key Laboratory of Brain and Cognitive Science, Institute of psychology, Chinese Academy of Sciences, Beijing 100101, China.

Department of Psychology, University of the Chinese Academy of Sciences, Beijing 100049, China

This article has been accepted for publication and undergone full peer review but has not been through the copyediting, typesetting, pagination and proofreading process, which may lead to differences between this version and the [Version of Record](#). Please cite this article as [doi: 10.1002/adhm.202200653](https://doi.org/10.1002/adhm.202200653).

This article is protected by copyright. All rights reserved.

J. Huang, Prof. Z. Li

College of Chemistry and Chemical Engineering, Guangxi University, Nanning 530004, China

Y.Q. Wang

College of Mechanical Engineering, Guangxi University, Nanning 530004, China

Y. Zhang

Department of Clinical Laboratory, Renmin Hospital of Wuhan University, WuHan, HuBei 430060, China

T. L. Yin

Reproductive Medicine Center, Renmin Hospital of Wuhan University, Wuhan, Hubei 430060, China. ,

Prof. Z. Li

Institute for Stem Cell and Regeneration, Chinese Academy of Sciences, Beijing 100101, China.

These authors contributed equally: Ying Liu, Chan Wang, Jiangtao Xue.

Corresponding authors: Tailang Yin (email: reproductive@whu.edu.cn) and Zhou Li (email: zli@binn.cas.cn)

### Abstract

Hydrogel-based epidermal electrodes have attracted widespread attention in health monitoring and human-machine interfaces for their good biocompatibility, skin-matched Young's modulus, and stable in situ electrophysiological recording performance. However, it is difficult to make the exact

conformal attachment between skin and electrodes because of the hair, wrinkles as well as complex, curved contours of the skin. This also results in signal distortion and large noise. Here, a body temperature enhanced skin-adhesive epidermal electrode is proposed based on non-covalent cross-linked network ionic hydrogel. The ionic hydrogel is fabricated by the polyvinyl alcohol (PVA), branched polyethyleneimine (b-PEI) and calcium chloride ( $\text{CaCl}_2$ ), which demonstrates impressive performances including ultra-stretchability of 1291 %, great adhesion to skin and other non-biological materials, stable conductivity of 3.09 S/m, recyclability and outstanding antibacterial ability, simultaneously. Specifically, the adhesion of the ionic hydrogel behaves as temperature-sensitive and could be enhanced by body temperature. Furthermore, the ionic hydrogel is utilized as epidermal electrodes, which displays seductive capability to record multifarious electrophysiological signals with high signal-to-noise ratio and ultra-low detection limit, including electrocardiogram (ECG), electromyogram (EMG) and electroencephalogram (EEG). The as-proposed body temperature enhanced skin-adhesive ionic hydrogel brings intelligent functions and broadens the way for epidermal electronics, promoting the development of healthcare electronics.

## 1. Introduction

Surface electrophysiological (EP) signals, represented by the electroencephalogram (EEG),<sup>[1]</sup> electrocardiogram (ECG)<sup>[2]</sup> and electromyogram (EMG),<sup>[3]</sup> contain various information about the health status of the human body. Highly efficient, precise and real-time recording of these EP signals is essential and significant in clinical diagnosis, monitoring and therapy.<sup>[4]</sup> The epidermal electrodes are attracting great attention for continuous and real-time transducing of these EP signals by forming an electrical interface with the skin in a portable and non-invasive approach.<sup>[1a, 5]</sup> Two important factors should be taken into consideration during this process. On the one hand, the EP signals are usually of small strength, instability, and randomness,<sup>[6]</sup> which places high requirements on the

epidermal electrodes during signal acquisition. On the other hand, it is difficult to form a conformal contact with low interfacial impedance between the epidermal electrodes and human skin, because the skin is physiological curved, soft, deformable and covered with hair and wrinkles.<sup>[7]</sup>

Numerous efforts have been made in developing advanced epidermal electrodes through improving mechanical properties,<sup>[5c, 8]</sup> electrical conductivity<sup>[5b]</sup> and interfacial interactions<sup>[9]</sup> with skin, which could be divided into dry electrodes and wet electrodes.<sup>[6]</sup> The dry electrodes are mainly based on metal particles, carbon materials and metallic nanomaterials and other materials such as conductive polymers.<sup>[4c]</sup> Although the dry electrodes exhibited outstanding performance in terms of electrical conductivity<sup>[6]</sup>, the weakness in stretchability, adhesion and tissue-mismatched modulus make them suffer from severe motion artifacts when acquiring surface physiological signals in motion.<sup>[4c, 6]</sup> Ionic hydrogels, as a typical example of wet electrodes, demonstrate the unique advantages with superior transparency,<sup>[10]</sup> stretchability,<sup>[11]</sup> tunable modulus,<sup>[12]</sup> biocompatibility<sup>[13]</sup> and biosimilar ionic conductivity<sup>[14]</sup> have attracted great interest.<sup>[5e, 15]</sup> Through the materials design,<sup>[16]</sup> the ionic hydrogel in tissue-matched modules enables conformal contact with human skin.<sup>[17]</sup> Meanwhile, the surface functional design of the ionic hydrogel enables strong surface interactions with human skin, based on physical interaction (i.e., hydrogen bonds, electrostatic interactions and host-guest interactions)<sup>[9, 18]</sup> and chemical interaction (i.e., Schiff's base reaction, C-H insertion and Michael addition),<sup>[9, 18b]</sup> which helps minimize the interfacial impedance.

Herein, we reported a multifunctional ionic hydrogel (MiH) which is equipped with body-temperature enhanced adhesion, stretchability, recyclability and antibacterial properties, simultaneously. The MiH built a dual physical cross-linked network with three components of polyvinyl alcohol (PVA), branched polyethyleneimine (b-PEI) and calcium chloride (CaCl<sub>2</sub>). In this ternary system, abundant hydrogen bonds and electrostatic interactions helped form robust adhesion

to skin and other non-biological materials. Meanwhile, under the comprehensive regulation of the content of  $\text{CaCl}_2$  and molecular weight of b-PEI, the optimal MiH displayed impressive performances, including ultra-stretchability of 1291 %, skin-matched modulus around 10 kPa and stable conductivity of 3.09 S/m. When applied as the epidermal electrode, the MiH built a highly compliant and gapless interface with the skin, enabling the real-time monitor of high-fidelity electrophysiological signals of EEG, ECG and EMG.

## 2. Results and Discussion

### 2.1. Design of the multifunctional ionic hydrogel (MiH)

Ionic hydrogel with skin adhesion has unique advantages in recording epidermal physiological signals.<sup>[5e]</sup> The skin-matched modulus, tight conformation adhesion to skin and biosimilar ionic conductivity make the epidermal electrodes based on ionic hydrogels possess a high signal-to-noise ratio and low detection limit in  $\mu\text{V}$ -scale during recording EPs (**Figure 1a**). We designed the multifunctional ionic hydrogel with skin-adhesive, stretchable and conductive properties for epidermal electrophysiological signals monitoring. The multifunctional ionic hydrogel was composed of PVA, b-PEI and  $\text{CaCl}_2$  based on a non-covalent cross-linked network. The hydrogen bonds formed by -OH in PVA and  $-\text{NH}_2$  in b-PEI help to construct the first network. After the introduction of  $\text{CaCl}_2$ , the coordination between hydroxyl (-OH)/amino ( $-\text{NH}_2$ ) and  $\text{Ca}^{2+}$  formed the second network (**Figure 1b**). These dynamic interactions endow hydrogels with large stretchability and modulus at the kPa-scale, which contributes to the conformal attachment on irregular surfaces. Additionally, the abundant polar groups of -OH,  $-\text{NH}_2$  among the multifunctional ionic hydrogel provide reversible adhesion through establishing hydrogen bonds and electrostatic interactions with the human skin.<sup>[19]</sup> Furtherly, the adhesion was enhanced over time to form a gapless contact based on the temperature-sensitive rheological properties of the non-covalent dynamic network and small molecules of b-PEI (**Figure**

1c).<sup>[20]</sup> Thus, the multifunctional ionic hydrogel achieved a much lower interfacial impedance by making a conformal contact with the skin based on the tissue-matched mechanical modules and enhanced adhesion.<sup>[5d]</sup>

## 2.2. Mechanical and electrical properties of the MiH

The mechanical properties, electrical conductivity and adhesion of ionic hydrogel could be comprehensively optimized by adjusting the content of  $\text{CaCl}_2$  and the molecular weight of b-PEI. As shown in **Figure 2a** and S1, we observed an increase in stretchability and decreased tendency in both strength and Young's modulus of the ionic hydrogel with the increase of the  $\text{CaCl}_2$  content. This phenomenon was mainly due to more -OH participated coordination bonds with  $\text{Ca}^{2+}$  and less in forming hydrogen bonds in the crystalline region, which was further confirmed by the X-Ray Diffraction spectrum (XRD) (Figure S2).<sup>[21]</sup> According to the Fourier transform infrared spectroscopy (FTIR), the wide absorption peaks centered around  $3300\text{ cm}^{-1}$  are attributed to the -OH stretching vibration. It shifted towards a higher wavenumber (from  $3269$  to  $3342\text{ cm}^{-1}$ ) with the increase of  $\text{CaCl}_2$ , indicating the coordination between  $\text{Ca}^{2+}$  and -OH (Figure S3).<sup>[22]</sup> Moreover, the larger molecular weight of b-PEI contributed to higher stretchability, strength and Young's modulus, satisfying more chain entanglement and physical cross-linking points in the network.<sup>[22]</sup> The stretchability, strength and modulus of these samples are located in the range of 308-1291 %, 93-129 kPa and 10-47 kPa, which could well adapt to the human skin with mechanical deformation within 15 %<sup>[4c]</sup> and the modulus of 0.1-1.95 MPa.<sup>[23]</sup>

The adhesion of the MiH was also affected by the content of  $\text{CaCl}_2$  and the molecular weight of b-PEI. As shown in Figure 2b, the adhesion of sample named 600-30% was far beyond others owing to the synergistic enhancement effect of more  $\text{Ca}^{2+}$  and smaller molecule b-PEI, which was selected for a further test (named MiH). The loading-rate-dependent tensile behavior of the MiH was studied and

Accepted Article

summarized in Figure 2c, indicating a gradually enhanced stretchability and tensile strength at the breakpoints with the loading speed increased from 50 to 500 mm/min. Moreover, the elastic recovery of the MiH from stretching to releasing states was investigated by multiple-stage cyclic tensile loading-unloading tests. At relatively low tensile strain (<500%), the stress-strain curves almost overlapped in the loading and unloading process (Figure 2d). As the tensile strain went beyond 500%, the hysteresis loops of stress-strain curves started to display obviously, which indicated the fracture and reversibility of hydrogen bonds and coordination bonds to dissipate energy under large deformation.<sup>[24]</sup> The MiH had only 33% residual strain after 10 loading-unloading cycles under the large deformation of 500% which showed great elasticity and mechanical recovery of MiH (Figure 2e).

The conductivity of the MiH was mainly related to the content of CaCl<sub>2</sub>. The Electrochemical Impedance Spectras (EIS, Figure 2f) showed a gradually reduced equivalent resistance (ER, calculated by the intersect with X-axis)<sup>[21]</sup> from 13.92 Ohm to 4.85 Ohm and an increased conductivity from 1.20 S/m to 3.09 S/m (Figure S4) along with the increasing of the CaCl<sub>2</sub>, for the more free ions participating in conductance. Considering the dynamic working environments (like on the skin), we explored the conductance stability of the ionic hydrogel under a large range of deformations, as shown in Figure 2g. Under the maximum feasible deformation of skin (about 15 %), the  $(R'-R_0)/R_0$  remained approximately 0.05, illustrating good working stability. To give a comprehensive presentation about stretchability, conductivity and adhesion, we connected the MiH into a circuit to replace a part of the wire(Figure 2h). The green light-emitting diode (LED) was lit successfully when closed the circuit (Figure 2h, i). When the MiH was stretched to 200 % to its original length, the brightness of LED just barely changed, indicating the stable conductivity under small deformation (ii). Cut the MiH into two parts and brought the separated parts together face to

face. The two pieces of ionic hydrogel connected the circuit based on the strong adhesion and the LED lit at once (iv, v).

### 2.3. Adhesive property of MiH

The MiH exhibited strong adhesion to various materials and complex physiological surfaces. When it adhered to the surface of the forearm, it did not detach or move under stretching, compressing and twisting (**Figure 3a**). The MiH also expressed conformal attachment to different complex physiological curves owing to its good mechanical adaptation and adhesion to the skin (Figure 3b). The 90-degree peel tests were performed on the volunteer's forearms to quantitatively assess the adhesion between skin and MiH, which demonstrates great adhesion performance with the adhesive interfacial toughness reached  $49 \text{ J/m}^2$  (Figure S5).<sup>[25]</sup> Additionally, the good transparency of MiH provided a clear view of skin states, which was significant in the clinical process. Furthermore, the MiH also exhibited good adhesion to other non-biological materials, which provided a direct bridge between the electronics and biological tissues. With the MiH as the middle layer, the glass bottle, PP tube, rubber stopper, Al cover, cotton roll and carton box were adhered steadily to the acrylic stick without falling (Figure 3c). To quantify the adhesion performance of the MiH, a standard 180-degree peel test, standard lap-shear test and standard tensile test were conducted to represent the interfacial toughness, shear strength and tensile strength, respectively (Figure 3d, 3e and 3f).<sup>[26]</sup> After calculation, we found that the MiH performed the best adhesion to the metal with interfacial toughness of  $861 \text{ J/m}^2$ , shear strength of  $18 \text{ kPa}$  and tensile strength of  $11.9 \text{ kPa}$ , respectively. Relatively, the adhesion of the ionic hydrogel to rubber, plastic and paper performed an attenuated tendency. The interfacial toughness, shear strength and tensile strength between the ionic hydrogel and the paper were calculated as the smallest, probably because the paper absorbed abundant moistures and resulted in little effective interactions on the interface.

## 2.4. The body-temperature enhanced adhesion of the MiH

The stable adhesion of the MiH is critical but also challenging when used as epidermal electrodes for the skin is constantly in a dynamic state and secreting oil and other secretions.<sup>[27]</sup> We adhered the MiH to the forearm of a volunteer and found them performed not only a stable contact but also an enhanced adhesion, as shown in **Figure 4a**. This phenomenon is mainly due to the higher temperature of the human body (about 36~37°C) compared with the environment (about 25°C) slowly heated the MiH, enabling tighter contact with skin. The infrared imager gave a clear exhibition that the temperatures of the adhered MiH, gradually increased from 28°C to 36°C (Figure 4b). To explore the rheological behavior of MiH along with the increased temperature more intuitively, we 3D-printed a micro-groove pattern substrate to simulate the wrinkles on the skin.<sup>[28]</sup> At 25°C, the MiH maintained its original planar shape, and the gaps between MiH and substrate were very clearly observed even after an hour (Figure S7). At 37°C, the MiH full-filled the microstructures of the substrate within 10 minutes (Figure 4c). The peel tests were performed on the skin of the volunteer's forearm to quantitatively characterized the adhesion at a different temperature which indicated that the interfacial toughness and adhesive energy improved gradually with the increased temperatures (Figure 4d, Figure S6). Furthermore, multiple characterizations of the rheological behavior of MiH confirmed our hypothesis. In the frequency sweep rheological measurement (Figure 4e), the storage modulus ( $G'$ ) was always larger than the loss modulus ( $G''$ ) during the whole frequency range at room temperature, indicating that the MiH has a stable cross-linked network in solid-state rather than the viscous fluid state.<sup>[29]</sup> Then, the mechanical modulus were evaluated by temperature sweep rheological measurement. As shown in Figure 4f,  $G'$  and  $G''$  gradually decreased with the increase of temperature and intersected at around 57°C, which was considered a sol-gel conversion point.<sup>[30]</sup> Figure 4f indicated the viscosity of the ionic hydrogel decreased with the increased temperature, which was

consistent with Figure 4h. In conclusion, the dynamic cross-linked network and the rheology of short polymer chains in the system enabled the MiH temperature-sensitive mechanical and adhesive properties. The body-temperature enhanced adhesive MiH would facilitate the formation of a long-term stable signal acquisition interface for the epidermal electrodes.

## 2.5. Applications for ECG and EMG recording

With the strong adhesion, high conductivity and tissue-matched modulus, the MiH made applications as epidermal electrodes to record the ECG and EMG signals (**Figure 5a**). For ECG signals recording, three pieces of MiH films all in size of  $3\times 3\times 1\text{cm}^3$  were used as epidermal electrodes, with two symmetrically adhered to two inner wrists of the volunteer as work electrodes and the third one placed on the right ankle as the ground electrode (Figure 5b). The ECG signals acquired by the MiH-based epidermal electrodes displayed distinct features of P waves, QRS waves and T waves, which are the basis to diagnose the function state of the heart in a clinical (Figure 5d).<sup>[2b]</sup> It's comparable to that of the commercial Ag/AgCl electrodes. Furthermore, the ECG signals from two volunteers of different genders during rest and after exercise were well-differentiated and recorded with the MiH electrodes, indicating a significant increase in heart rate after exercise (Figure 5e).

EMG is another important electrophysiological signal related to health status. For EMG recording, as shown in Figure 5c, two pieces of MiH films were attached to the forearm as working electrodes, and another one behaved as the reference electrode was placed at the back of the elbow joint. As shown in Figure 5f, the ionic hydrogel epidermal electrodes successfully collected the EMG signals induced by muscles during arm movements, exhibiting lower interface resistance and higher signal-to-noise ratio (SNR=8.5) than commercial Ag/AgCl electrodes (SNR=6.4). Figure 5g presented the EMG signals generated by muscle groups in the forearm at different gripping forces.<sup>[5b]</sup> With the grip

strength increased from 100 to 600 N, the peak-to-peak amplitude and duration of a single EMG signal rose steady, indicating larger grip force might require more muscle bundles to contract and spent longer time to recover to the original state (Figure 5h, 5i). Furtherly, we also recorded the EMG signals during the upper arm training in lifting the dumbbell (Figure 5j). The EMG signals indicated that the muscles contractions happened during raising, holding and downing arm with loading. Increasing the weight of dumbbells, the amplitude of EMG signals grew larger, which indicated that the muscles work harder to overcome the weight of the heavier dumbbells (Figure 5k).<sup>[5c]</sup>

## 2.6. Application for EEG recording

EEG signals are significant for the diagnosis and therapy the brain diseases.<sup>[4c]</sup> Compared with ECG and EMG, recording high-quality EEG signals is much more challenging due to the weak epidermal potential ( $\mu\text{V}$  scale) and the large background noise.<sup>[5a]</sup> To collect the EEG signals in the area of the frontal lobe, MiHs were used as conductive interfaces to connect electrodes and the scalp. Three pieces of MiH were mounted at Fp1, Fpz and Fp2 sites of wireless EEG acquisition system, and the Pz and AFz sites were used as ground electrode and reference electrode, respectively (**Figure 6a** and **6b**). As shown in **Figure 6c**, the epidermal electrodes recorded the EEG signals of the tested volunteer in both test and non-test conditions. Compared to the non-test state, the EEG signals during the test state were more stable because the volunteer was in a state of heighten concentration. After removing the signals from eyes movements, we obtained the P300 signals through superimposing and averaging three channels EEG signals from Fp1, Fpz and Fp2 sites (**Figure 6d**).<sup>[31]</sup> After the target stimulation was applied from the P300 speller, the volunteer generated typical P300 peaks (**Figure 6d** and **e**).<sup>[31]</sup> Furtherly, through the fast Fourier transformation (FFT) analysis, the delta wave (0.5-4.0 Hz) and theta wave (4.0-7.5 Hz) were extracted from the original P300 signals, which was related to the cognitive function of the brain (**Figure 6f, g** and **h**). Moreover, this EEG test was also carried out

using a commercial conductive gel as a comparison, more details could be found in Figure S8. In conclusion, the MiH demonstrated great potential as epidermal electrodes for the physiological signals recording and promoted the development of physiological health monitoring and diagnosis system.

## 2.7. Recyclable, antibacterial properties of the ionic hydrogel

The development of recyclable materials provided a promising avenue to tackle electronic waste pollution.<sup>[24, 32]</sup> Based on the non-covalent cross-linked network, the MiH was sensitive to temperature and could take place gel-sol transition at 57°C. This provided a basis for remodeling temperature. To investigate the recyclability of the MiH, the tested samples were cut into pieces and then transformed into sol through heating over 57°C in a water bath, which was furtherly modeled into desired shapes (Figure 7a, Figure S9). As shown in Figure 7b, the mechanical properties of the recycled MiH were almost identical to the original sample. The tensile strain-stress curves of the samples performed similar shape and same tensile strength/maximum deformation at the break.<sup>[24]</sup> The loading-unloading test also confirmed the good recovery of the recycled MiH. Additionally, the conductivity of recycled MiH could recover 92% of the original sample, showing the recycled MiH still had a high conductivity (Figure 7c, Figure S10).<sup>[33]</sup> Thus, it could be concluded that the MiH is feasible to replace single-use electronics.

After that, the antibacterial properties of the ionic hydrogel were explored. The *Escherichia coli* (*E. coli*) and *Staphylococcus aureus* (*S. aureus*) were used to examine the antibacterial property in the fluid culture mediums. As shown in Figure 7d, there were almost no *E. coli* and *S. aureus* survived in the experimental groups (named PEI and MiH) after coculture for 18 h at 37°C compared with the blank group and control group (named PVA). The outstanding antibacterial efficiency comes from the positive-charged PEI, which absorbed the positively bacterial biofilm and induced the rupture of the bacterial biofilm, resulting in bacterial death<sup>[15a, 34]</sup>

Figures

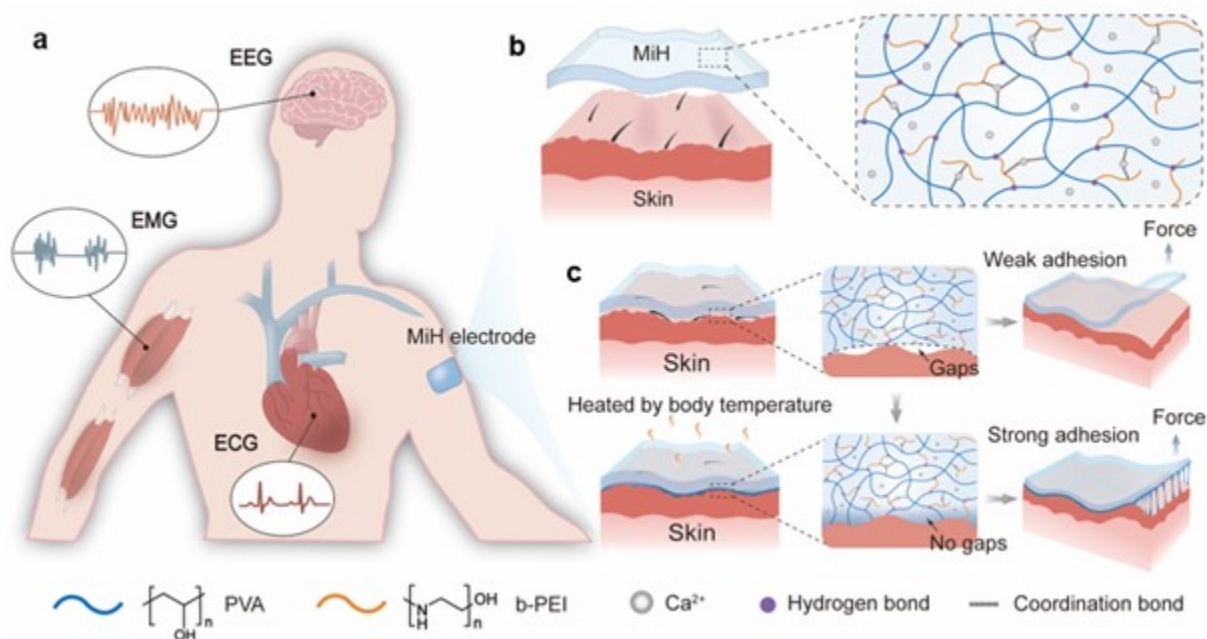


**Figure 1.** Schematic illustration of the multifunctional ionic hydrogel (MiH) epidermal electrode for monitoring electrophysiological signals. (a) The schema of electrophysiological signals (EEG, EMG and ECG). (b) The design principle of the MiH. (c) The schematic illustration of the body temperature enhanced adhesion of MiH.

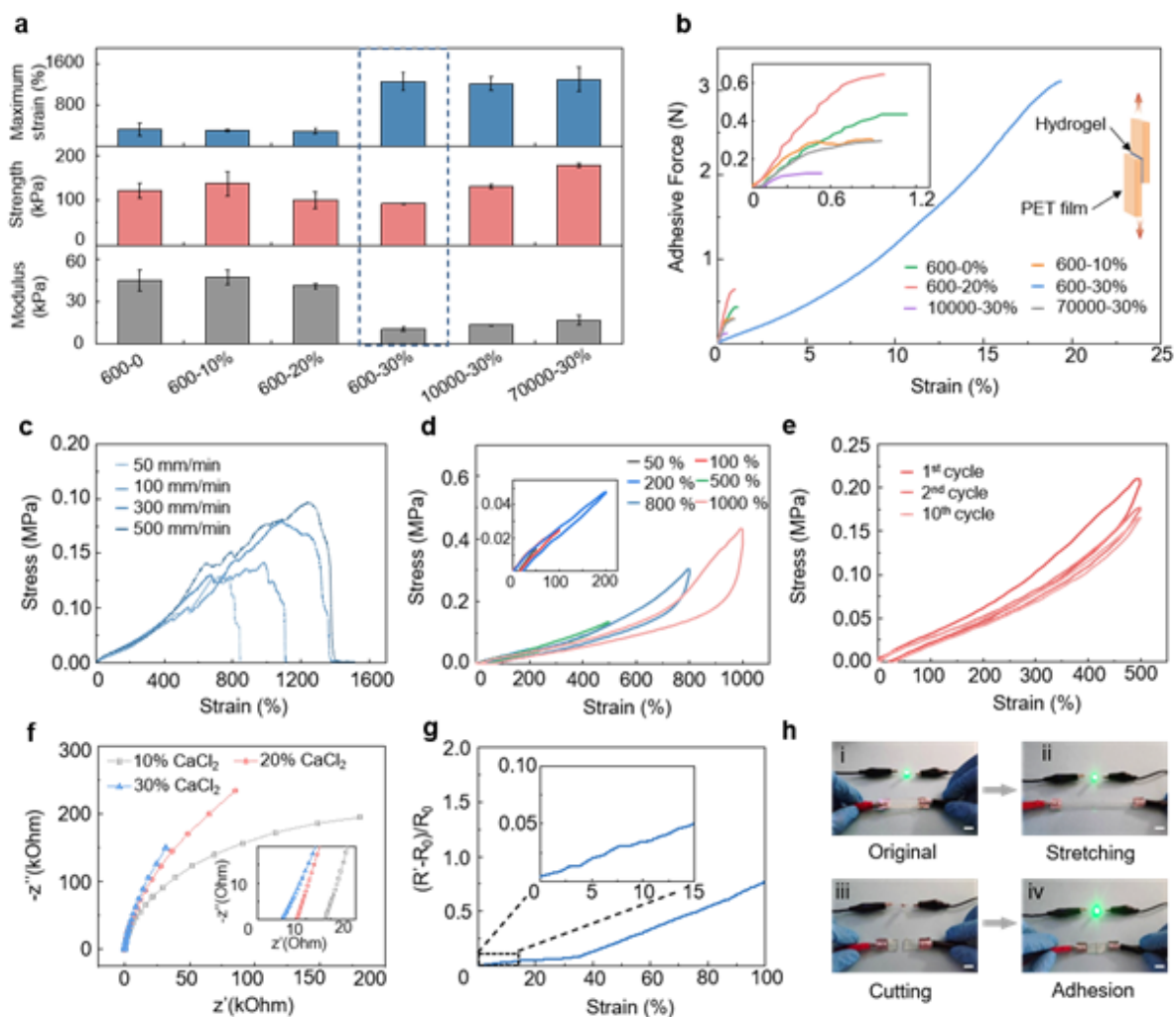


**Figure 2.** Mechanical, adhesive and electrical properties optimization of the MiH. (a) The strain, strength and modulus of the ionic hydrogel with different  $\text{CaCl}_2$  content (10 %, 20 % and 30 %) and different molecular weight of b-PEI (600, 10000 and 70000). (b) The adhesion of the ionic hydrogel with different  $\text{CaCl}_2$  content and b-PEI molecular weight. (c) Tensile stress-strain curves of the MiH with loading rate ranged from 50 mm/min to 500 mm/min. (d) Cyclic tensile loading-unloading curves of the MiH with different tensile deformation (50%, 100%, 200%, 500%, 800% and 1000%) and (e) different cycle times (1<sup>st</sup>, 2<sup>nd</sup> and 10<sup>th</sup>) at 500% strain. (f) The electrochemical impedance spectra (EIS) of the ionic hydrogel with 10 %, 20 % and 30 %  $\text{CaCl}_2$ . (g) The resistance of the MiH

changed along with strain. (h) The MiH as a conductor assembled in a circuit with a green LED bulb. Stretching-cutting-adhesion test confirmed the stable conductivity of the MiH. Scale bar: 1 cm.

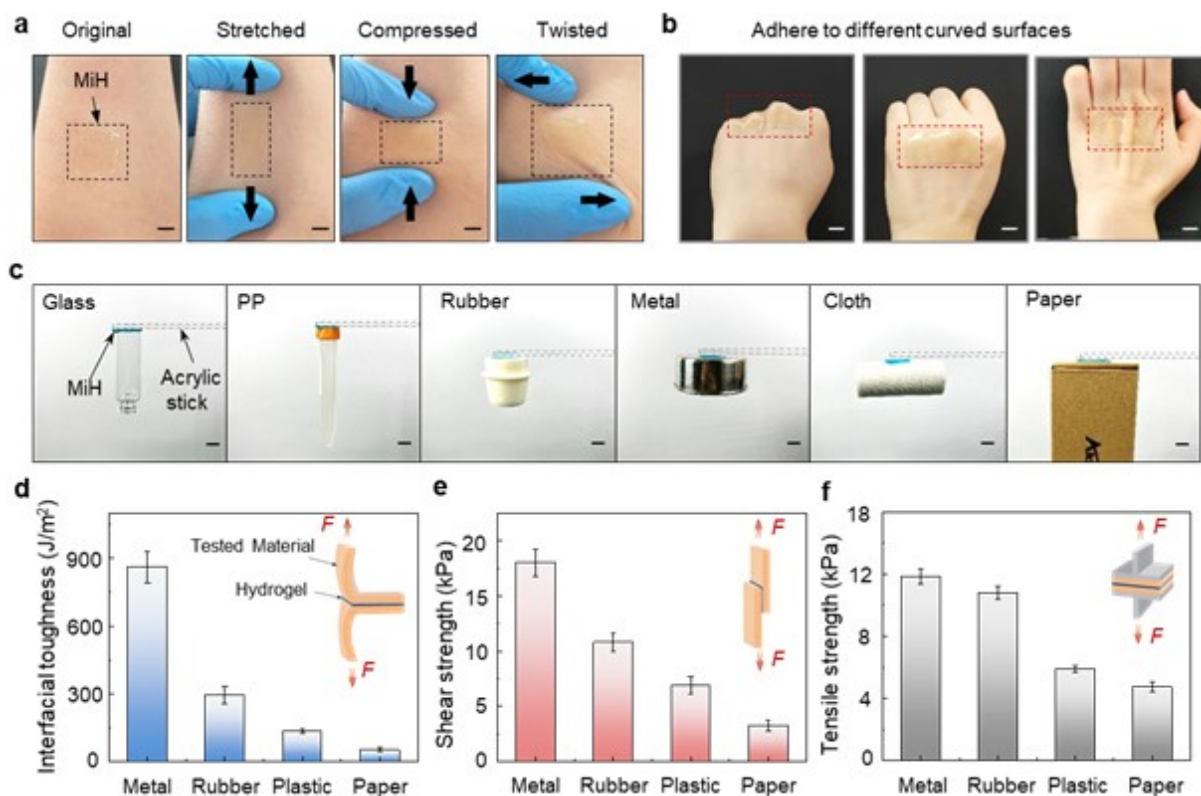


**Figure 3.** The adhesive property of the MiH. (a) MiH was attached to the forearm in its original, stretched, compressed and twisted state. Scale bar: 1 cm. (b) The MiH made a conformal adhesion to complex curves. Scale bar: 1 cm. (c) Photographs of MiH adhered to various material surfaces. Scale bar: 1 cm. (d) The interface toughness, (e) shear strength and (f) tensile strength of adhesion between MiH and different materials.

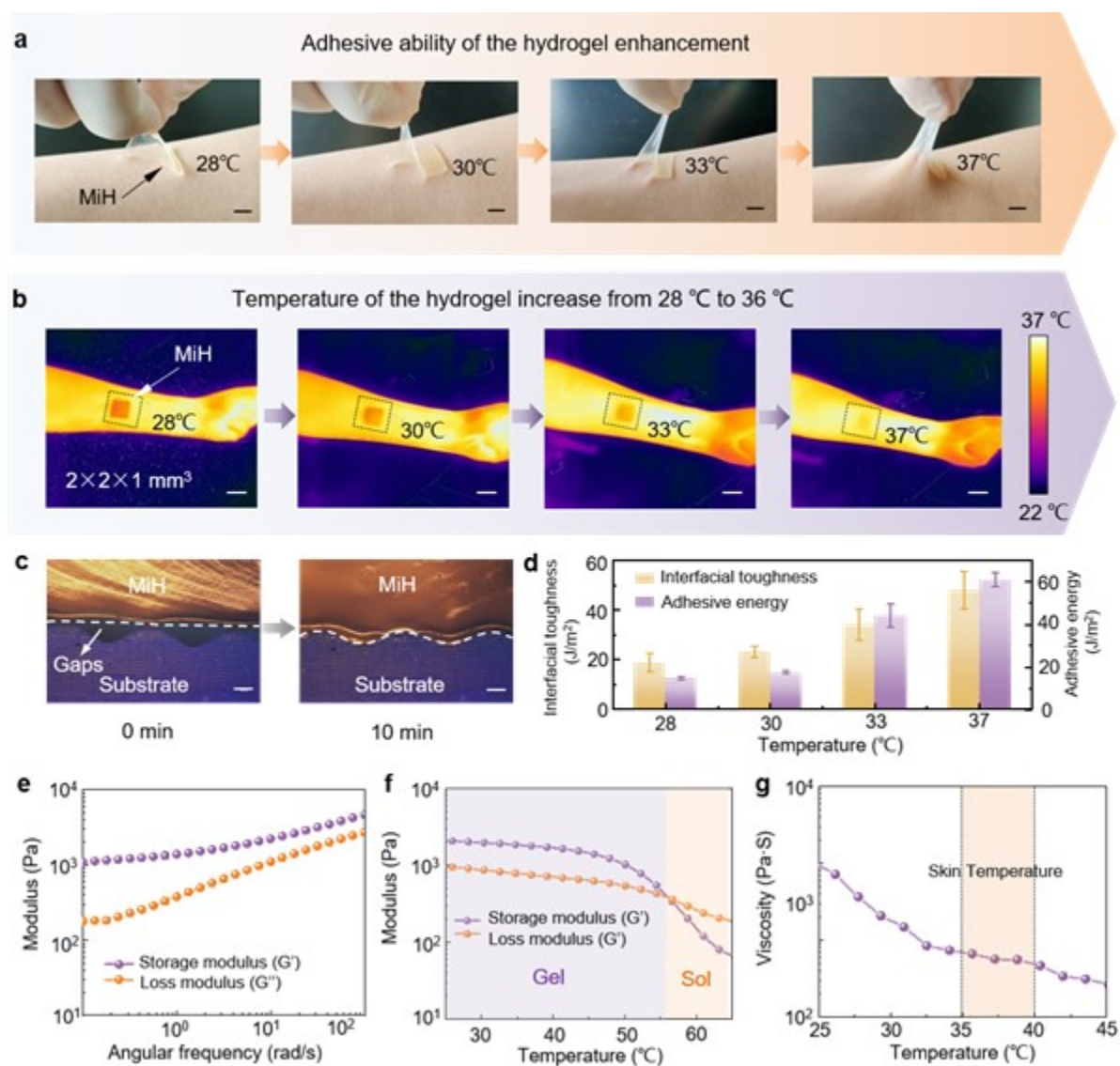


**Figure 4.** The body-temperature enhanced adhesion of the MiH. (a) The adhesion of the MiH was enhanced by the skin temperature. Scale bar: 1 cm. (b) Infrared thermal images of MiH adhered on the forearm. The temperature of MiH gradually increased to near that of the skin. Scale bar: 4 cm. (c) Microscope images of MiH placed on the micro-grooved substrate at 37°C. Scale bar: 200  $\mu\text{m}$ . (d) The interfacial toughness and adhesive energy of skin and MiH at different temperatures. (e) Frequency-dependent oscillatory rheology of MiH from 0.1 to 100 rad/s at 25 °C, with strain=1 %. (f) Temperature-dependent oscillatory rheology of MiH from 30 to 60 °C with strain=1 %,  $\omega=10$  rad/s. (g) Viscosity tests of MiH with temperature from 25°C to 45°C.

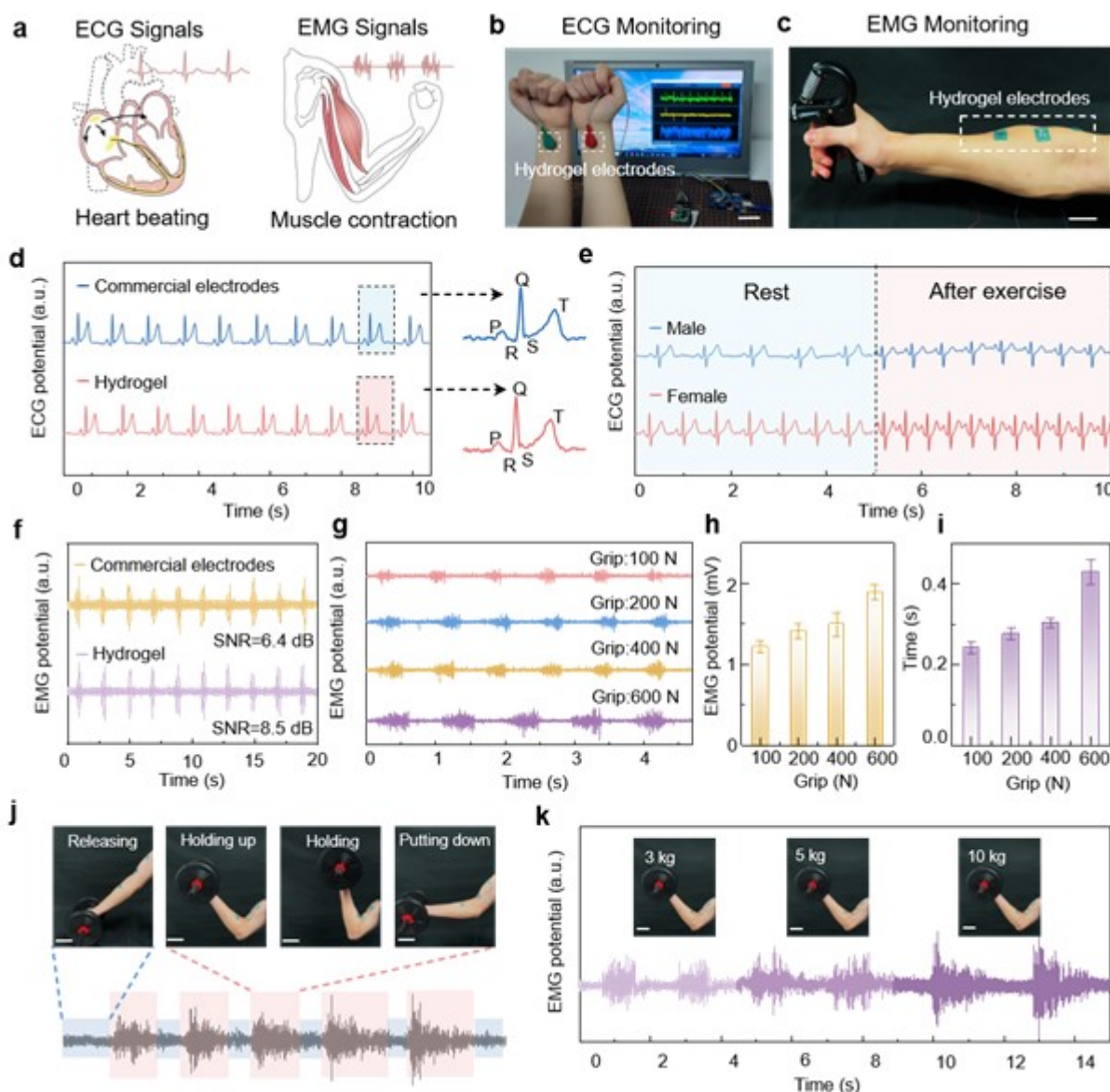
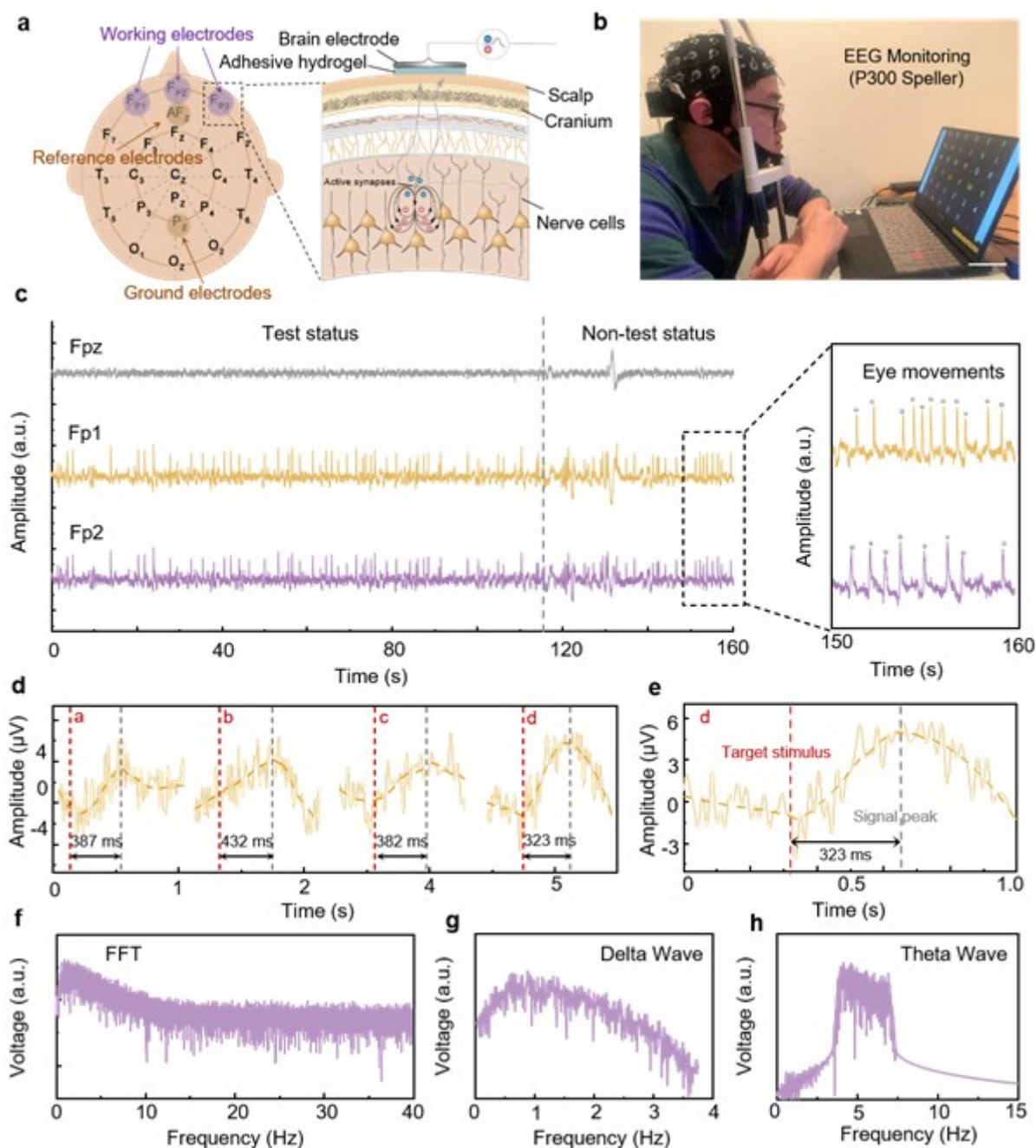


**Figure 5.** EMG and ECG recording using MiH epidermal electrodes. (a) The schematic diagram of EMG and ECG. (b) MiH epidermal electrodes for ECG monitoring. (c) MiH epidermal electrodes for EMG monitoring. (d) The ECG signals were recorded by MiH epidermal electrodes and commercial electrodes. (e) ECG signals of a male and female in rest and after exercise. (f) EMG signals were measured by commercial electrodes and MiH. (g) EMG signals during gripping a dynamometer with different forces. (h) EMG potential intensity (peak-to-peak value) under different gripping forces. (i) Duration of the EMG signal under different gripping forces. (j) EMG signals during the action of

lifting 10 kg dumbbells and the corresponding images. Scale bar: 8 cm. (k) EMG signals during lifting dumbbell with different weights and the corresponding images (inset). Scale bar: 8 cm.



This article is protected by copyright. All rights reserved.

**Figure 6.** MiH epidermal electrode for EEG monitoring. (a, b) The schematic diagram of EEG monitoring with MiH. Scale bar: 10 cm. (c) EEG signals of the Fp1, Fp2 and Fpz sites. (d) The extracted P300 signals. The red dotted lines represent the target simulation. (e) Single P300 signal. (f) Fast Fourier Transformed EEG signals. (g) The extracted delta wave and (h) theta wave.

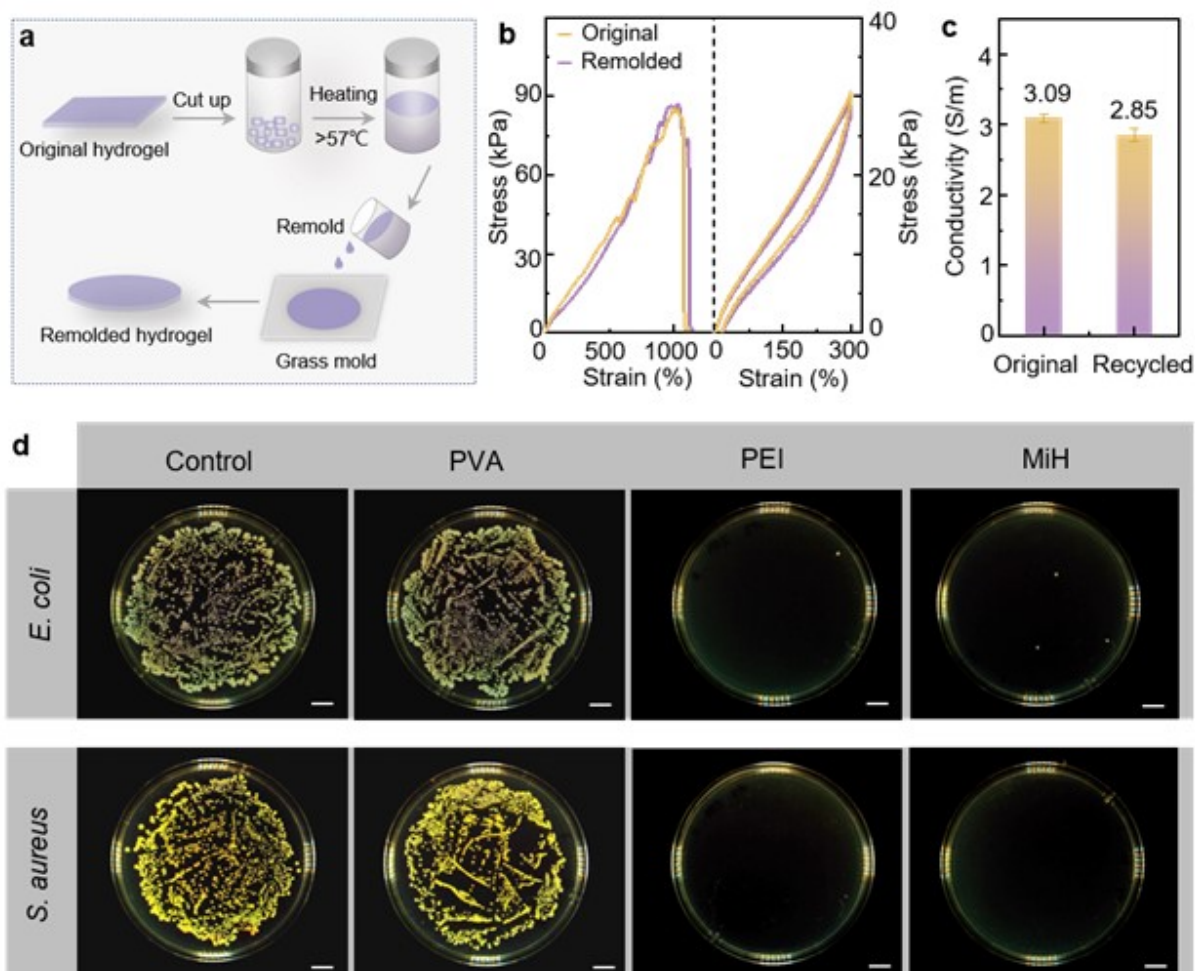


**Figure 7.** Recyclable and antibacterial properties of the MiH. (a) The schematic diagram of MiH recyclability. (b) The tensile test and recovery ability of the original and recycled MiH. (c) The conductivity of hydrogel before and after remolding. (d) Photographs of *E. coli* and *S.aureus* after coculturing with the composite samples: i) control; ii) PVA; iii) PEI ; vi) MiH. Scale bar: 1 cm.

### 3. Conclusion

In summary, we developed a multifunctional ionic hydrogel (MiH) with body temperature enhanced adhesion for epidermal electrodes in physiology monitoring. Firstly, we designed and fabricated the ternary ionic hydrogel consisting of biofriendly PVA, b-PEI and  $\text{CaCl}_2$  through harmoniously constructing a non-covalent cross-linked network. By regulating the concentration of  $\text{CaCl}_2$  and the molecular weight of b-PEI, we obtained the MiH with optimal stretchability of 1291%, the electrical conductivity of 3.09 S/m and strong adhesion with skin and other non-biological materials. In particular, the adhesion was temperature-sensitive and could be enhanced by body temperature, which is favorable for establishing a long stable conformal interface with skin. Then, the MiH made applications as epidermal electrodes, hehaving outstanding monitoring capability with a high signal-to-noise ratio and low detection limit for various physiological signals. The epidermal electrodes clearly distinguished the difference in ECG signals between male and female volunteers during rest or after exercise. When the volunteer increased the grip strength from 100 N to 600 N, the corresponding intensity of the EMG signals rose from 1.2 to 1.9 mV. In EEG monitoring, the MiH epidermal electrodes successfully captured P300 signals as well as the typical delta and theta waves.

The MiH guaranteed the high signal-to-noise ratio and low detection limit through establishing a long-term stable interface with skin based on its: i) the tissue-matched modulus; ii) non-destructive

and strong adhesion to human skin; iii) high electrical conductivity. With the positively charged b-PEI, the MiH showed a high antibacterial effect against *E. coli* and *S. aureus*, avoiding the risk of sore infection in clinical patients. Finally, after service, the MiH could be reused, which contributes to reducing pollution and facilitating carbon neutralization. Given the above, we believe the multifunctional ionic hydrogel will bring intelligent functions and broaden the way for epidermal electronics, promoting the development of healthcare electronics.

#### 4. Experimental Section

*Preparation of hydrogels:* Hydrogels were synthesized by one-pot and freezing/thawing method. Specifically, moderate (10, 20 and 30 wt %)  $\text{CaCl}_2$  (CAS: 20150703, BEIJING SHIJI, Beijing, China), 1.0 g polyethyleneimine (b-PEI, CAS: 9002-98-6, MW = 600, 10000 and 70000, Aladdin, Shanghai, China) and 2.0 g polyvinyl alcohol (PVA, CAS: 9002-89-5, 1799, Aladdin) were dissolved in 9.0 ml of deionized water successively to form a homogeneous solution in a water bath of 98°C under continuous magnetic stirring for 1-2 h. Then the uniform sol was shaped into a thin film in glass mold to freeze at -20°C for 12 h and then thawed at 25°C for 6 h.

*Recycling of MiH:* To evaluate the recyclability and remodeling of the MiH, they were placed in glass bottles and heated in a water bath at 85°C until the solid hydrogels transformed into a uniform solution. And then, the redissolved samples were poured into a mold to reshape and placed at -20°C for 12 h, followed by thawing at 25°C for 6 h to regain the hydrogels.

*Material Characterizations:* The tensile tests of hydrogels were performed on the ESM301/Mark-10 system (Mark-10 Corporation, New York, NY, USA) and the stretching rate is 50  $\text{mm}\cdot\text{min}^{-1}$ . The

Accepted Article

samples for the tensile test had a size of  $20 \times 10 \times 2 \text{ mm}^3$ . The oscillatory rheology and viscosity of hydrogels were performed by the MCR92 rheometer (Anton Paar, Shanghai, China). Fourier transform infrared spectroscopy (FTIR) was obtained using a VERTEX80v spectrometer (Bruker, Karlsruhe, Germany). X-ray diffraction (XRD) was performed using PANalytical X'Pert3 Power with  $2\theta$  ranging from  $10^\circ$  to  $60^\circ$ , where Cu K $\alpha$  radiation ( $\lambda=1.5406 \text{ \AA}$ ) was operated at 40 kV and 40 mA. Raman spectroscopy was performed by LABRAM HR EVOLUTION spectrometer (HORIBA JY, France). The temperature of MiH adhered to the skin surface of the forearm was measured by an Infrared thermal imager (FLIR ONE, America).

*Adhesion of hydrogels:* To measure interfacial toughness, the hydrogel samples with widths of 2 cm were adhered to the substrates and tested by the standard 180-degree peel test (ASTM F2256). As the peeling process reached a steady state, the measured force entered a plateau. The interface toughness was determined by dividing two times the plateau force. To measure shear strength, adhered samples with an area of  $2 \times 2 \text{ cm}^2$  were tested by the standard lap-shear test (ASTMF2255). The shear strength was determined by dividing the maximum force by the adhesion area. To measure tensile strength, adhered samples with an area of  $2 \times 2 \text{ cm}^2$  were tested by the standard tensile test (ASTMF2258). The tensile strength was determined by dividing the maximum force by the adhesion area. Plastic fixtures by 3D printed were applied using cyanoacrylate glues to provide grips for tests. All samples with size of  $2 \times 2 \times 1 \text{ cm}^3$  were performed by the mechanical testing machine (ESM301/Mark-10 system) with a constant tensile speed of  $50 \text{ mm} \cdot \text{min}^{-1}$ .

*Electrical Measurements:* The electrochemical impedance spectroscopy (EIS) tests of the hydrogels were tested by an electrochemical workstation (CHI 650E, Chenhua, Shanghai, China). The EIS was

performed at an open circuit at a range of 1 MHz to 0.1 Hz. The real-time current/resistance change of hydrogel under different deformations was measured by a Keithley 6517 electrometer, and the data was collected and recorded by an oscilloscope (LeCroy HDO6104).

*Electrophysiological monitoring:* The EMG signals were acquired by adhesive hydrogel electrodes and commercial electrodes (Ag/AgCl) which were connected to a Lead wire type two-lead EMG module (ED0136/EDK0056) and recorded by an oscilloscope (LeCroy HDO6104). The ECG signals were monitored using the ECG acquisition module (ADS1293) and recorded by PROCESS software. The EEG signals were tested by a 64-lead wireless EEG acquisition system (Neuraacle, NeuSen W) with MiH and commercial conductive gel (COMPUMEDICS NeuroMedical Supplies). The EEG signal processing was performed on the collected data using MATLAB for fundamental signal analysis (Independent Component Analysis / Superposition Average / Fast-Fourier Transform / Filter).

*Antibacterial studies:* The bacteria solution ( $10^6$  CFU mL<sup>-1</sup>) was prepared according to the method we reported previously. Three kinds of samples (PVA, PEI, and PVA-PEI-CaCl<sub>2</sub>) were added into *E. coli* and *S. aureus* solution (mass ratio of 1:20), respectively, and then co-cultured at 37°C for 18 h. In particular, the group which was added nothing to the bacteria solution was set as control. After co-cultivation, 100 µl of bacterial suspensions were pipetted from each group and spread onto the agar plates. In the end, these agar plates were kept in a constant temperature incubator at 37°C, after 18 h, the bacterial growth in agar plates was observed.

### Supporting Information

Supporting Information is available from the Wiley Online Library or the author.

**Acknowledgments**

This study was supported by the National Natural Science Foundation of China (61875015, T2125003), the Strategic Priority Research Program of the Chinese Academy of Sciences (XDA16021101), the Beijing Natural Science Foundation (JQ20038, L212010).

**References\***

- [1] a) L.R. Hochberg, D. Bacher, B. Jarosiewicz, N.Y. Masse, J.D. Simeral, J. Vogel, S. Haddadin, J. Liu, S.S. Cash, P. van der Smagt, J.P. Donoghue, *Nature*. **2012**, 485, 372-5; b) H. Yuk, B. Lu, S. Lin, K. Qu, J. Xu, J. Luo, X. Zhao, *Nat. Commun.* **2020**, 11, 1604.
- [2] a) J. Liu, X. Zhang, Y. Liu, M. Rodrigo, P.D. Loftus, J. Aparicio-Valenzuela, J. Zheng, T. Pong, K.J. Cyr, M. Babakhanian, J. Hasi, J. Li, Y. Jiang, C.J. Kenney, P.J. Wang, A.M. Lee, Z. Bao, *Proc. Natl. Acad. Sci.* **2020**, 117, 14769-14778; b) H. Ouyang, Z. Liu, N. Li, B. Shi, Y. Zou, F. Xie, Y. Ma, Z. Li, H. Li, Q. Zheng, X. Qu, Y. Fan, Z.L. Wang, H. Zhang, Z. Li, *Nat. Commun.* **2019**, 10, 1821.
- [3] a) M.C. Stanisa Raspopovic, Francesco Maria Petrini, Marco Bonizzato, Jacopo Rigosa, Giovanni Di Pino, Jacopo Carpaneto, Marco Controzzi, Tim Boretius, Eduardo Fernandez, Giuseppe Granata, Calogero Maria Oddo, Luca Citi, Anna Lisa Ciancio, Christian Cipriani, Maria Chiara Carrozza, Winnie Jensen, Eugenio Guglielmelli, Thomas Stieglitz, Paolo Maria Rossini, Silvestro Micera, *Sci. Transl. Med.* **2014**, 6, 222ra19-222ra19; b) G. Gu, N. Zhang, H. Xu, S. Lin, Y. Yu, G. Chai, L. Ge, H. Yang, Q. Shao, X. Sheng, X. Zhu, X. Zhao, *Nat. Biomed. Eng.* **2021**, 1-10.
- [4] a) J.M. B. J. Edelman, D. Suma, C. Zurn, E. Nagarajan, B. S. Baxter, C. C. Cline, B. He, *Sci. Robot.* **2019**, 4, eaaw6844; b) R.A. Nawrocki, H. Jin, S. Lee, T. Yokota, M. Sekino, T. Someya, *Adv. Funct. Mater.* **2018**, 28, 1803279. c) H. Wu, G. Yang, K. Zhu, S. Liu, W. Guo, Z. Jiang, Z. Li, *Adv. Sci.* **2021**, 8, 2001938.
- [5] a) Y. Zhao, S. Zhang, T. Yu, Y. Zhang, G. Ye, H. Cui, C. He, W. Jiang, Y. Zhai, C. Lu, X. Gu, N. Liu, *Nat. Commun.* **2021**, 12, 4880; b) L. Zhang, K.S. Kumar, H. He, C.J. Cai, X. He, H. Gao, S. Yue, C. Li, R.C. Seet, H. Ren, J. Ouyang, *Nat. Commun.* **2020**, 11, 4683; c) P. Tan, H. Wang, F. Xiao, X. Lu, W. Shang, X.

Deng, H. Song, Z. Xu, J. Cao, T. Gan, B. Wang, X. Zhou, *Nat. Commun.* **2022**, 13, 358; d) L. Pan, P. Cai, L. Mei, Y. Cheng, Y. Zeng, M. Wang, T. Wang, Y. Jiang, B. Ji, D. Li, X. Chen, *Adv. Mater.* **2020**, 32, e2003723; e) C. Yang, Z. Suo, *Nat. Rev. Mater.* **2018**, 3, 125-142.

[6] a) Y. Fu, J. Zhao, Y. Dong, X. Wang, *Sensors* **2020**, 20, 3651; b) Y. Shi, R. Liu, L. He, H. Feng, Y. Li, Z. Li, *Smart Materials in Medicine* **2020**, 1, 131-147.

[7] N.G. Jablonski, *Annual Review of Anthropology* **2004**, 33, 585-623.

[8] G. Ye, J. Qiu, X. Fang, T. Yu, Y. Xie, Y. Zhao, D. Yan, C. He, N. Liu, *Mater. Horiz.* **2021**, 8, 1047-1057.

[9] J. Yang, R. Bai, B. Chen, Z. Suo, *Adv. Funct. Mater.* **2019**, 30, 1901693.

[10] a) Z. Yu, P. Wu, *Adv. Mater.* **2021**, 33, e2008479; b) Z. Yu, P. Wu, *Mater. Horiz.* **2021**, 8, 2057-2064.

[11] X. Qu, S. Wang, Y. Zhao, H. Huang, Q. Wang, J. Shao, W. Wang, X. Dong, *Chem. Eng. J.* **2021**, 425, 131523.

[12] a) G.Z. Junsoo Kim, Meixuanzi Shi, Zhigang Suo, *Science*. **2021**, 374, 212-216; b) G.Z. Junsoo Kim, Meixuanzi Shi, Zhigang Suo, *Science*. **2021**, 374, 212-216

[13] a) ; b) R. Huang, X. Zhang, W. Li, L. Shang, H. Wang, Y. Zhao, *Adv. Sci.* **2021**, 8, e2100201; c) X. Chen, J. Zhang, K. Wu, X. Wu, J. Tang, S. Cui, D. Cao, R. Liu, C. Peng, L. Yu, J. Ding, *Small Methods*. **2020**, 4, 2000310.

[14] H. Yuk, B. Lu, X. Zhao, *Chem. Soc. Rev.* **2019**, 48, 1642-1667.

[15] a) C. Wang, K. Hu, C. Zhao, Y. Zou, Y. Liu, X. Qu, D. Jiang, Z. Li, M.R. Zhang, Z. Li, *Small*. **2020**, 16, e1904758; b) C. Wang, X. Qu, Q. Zheng, Y. Liu, P. Tan, B. Shi, H. Ouyang, S. Chao, Y. Zou, C. Zhao, Z. Liu, Y. Li, Z. Li, *ACS Nano*. **2021**, 15, 10130-10140.

[16] A. Jayakumar, V.K. Jose, J.M. Lee, *Small Methods*, 2020, 4, 1900735.

- [17] a) D. Gan, W. Xing, L. Jiang, J. Fang, C. Zhao, F. Ren, L. Fang, K. Wang, X. Lu, *Nat. Commun.* **2019**, 10, 1487; b) J. Luo, J. Yang, X. Zheng, X. Ke, Y. Chen, H. Tan, J. Li, *Adv. Healthc. Mater.* **2020**, 9, e1901423.
- [18] a) G. Bovone, O.Y. Dudaryeva, B. Marco-Dufort, M.W. Tibbitt, *ACS Biomater. Sci. Eng.* **2021**, 7, 4048-4076; b) X. Liu, H. Yu, L. Wang, Z. Huang, F. Haq, L. Teng, M. Jin, B. Ding, *Adv. Mater. Interfaces* **2021**, 9, 2101038; c) Y. Xiong, X. Zhang, X. Ma, W. Wang, F. Yan, X. Zhao, X. Chu, W. Xu, C. Sun, *Polym. Chem.* **2021**, 12, 3721-3739.
- [19] C. Heinzmann, C. Weder, L.M. de Espinosa, *Chem. Soc. Rev.* **2016**, 45, 342-358.
- [20] J. Huang, Y. Xu, S. Qi, J. Zhou, W. Shi, T. Zhao, M. Liu, *Nat. Commun.* **2021**, 12, 3610.
- [21] C. Wang, Y. Liu, X. Qu, B. Shi, Q. Zheng, X. Lin, S. Chao, C. Wang, J. Zhou, Y. Sun, G. Mao, Z. Li, *Adv. Mater.* **2022**, e2105416.
- [22] a) D.A. Leigh, F. Schaufelberger, L. Pirvu, J.H. Stenlid, D.P. August, J. Segard, *Nature.* **2020**, 584, 562-568; b) Q. Lian, H. Chen, Y. Luo, Y. Li, J. Cheng, Y. Liu, *Polymer.* **2022**, 247, 124754.
- [23] A. Ni Annaidh, K. Bruyere, M. Destrade, M.D. Gilchrist, M. Ottenio, *J. Mech. Behav. Biomed. Mater.* **2012**, 5, 139-148.
- [24] H. Wang, J. Lu, H. Huang, S. Fang, M. Zubair, Z. Peng, *J. Colloid Interface Sci.* **2021**, 588, 295-304.
- [25] G. Bao, R. Huo, Z. Ma, M. Strong, A. Valiei, S. Jiang, S. Liu, L. Mongeau, J. Li, *ACS Appl. Mater. Interfaces.* **2021**, 13, 37849-37861.
- [26] H. Yuk, C.E. Varela, C.S. Nabzdyk, X. Mao, R.F. Padera, E.T. Roche, X. Zhao, *Nature.* **2019**, 575, 169-174.
- [27] K. He, Z. Liu, C. Wan, Y. Jiang, T. Wang, M. Wang, F. Zhang, Y. Liu, L. Pan, M. Xiao, H. Yang, X. Chen, *Adv. Mater.* **2020**, 32, e2001130.
- [28] a) E. Decencière, A. Belhedi, S. Koudoro, F. Flament, G. François, V. Rubert, I. Pécile, J. Pierre, *Image Anal. Stereol.* **2019**, 38; b) J. Genzer, J. Groenewold, *Soft Matter.* **2006**, 2, 310-323.

- [29] Y. Wu, D.U. Shah, C. Liu, Z. Yu, J. Liu, X. Ren, M.J. Rowland, C. Abell, M.H. Ramage, O.A. Scherman, *Proc. Natl. Acad. Sci.* **2017**, 114, 8163-8168.
- [30] Rwei S. P., T. Y. Chen, and Y. Y. Cheng, *J. Biomater. Sci. Polymer Edn.* **2005**, 16, 1433–1445.
- [31] Y.L. Jiahui Pan, Tianyou Yu, *APSIPA ASC 2011 Xi'an.* **2011**.
- [32] L. Fan, J. Xie, Y. Zheng, D. Wei, D. Yao, J. Zhang, T. Zhang, *ACS Appl. Mater. Interfaces.* **2020**, 12, 22225-22236.
- [33] a) Y. Gao, S. Gu, F. Jia, G. Gao, *J. Mater. Chem. A* **2020**, 8, 24175-24183; b) Lai JL, Zhou HW, Wang MC, *J. Mater. Chem. C* **2018**, 6: 13316-13324.
- [34] a) J. Tian, H. Feng, L. Yan, M. Yu, H. Ouyang, H. Li, W. Jiang, Y. Jin, G. Zhu, Z. Li, Z.L. Wang, *Nano Energy.* **2017**, 36, 241-249; b) G. Wang, H. Feng, L. Hu, W. Jin, Q. Hao, A. Gao, X. Peng, W. Li, K.Y. Wong, H. Wang, Z. Li, P.K. Chu, *Nat. Commun.* **2018**, 9, 2055.

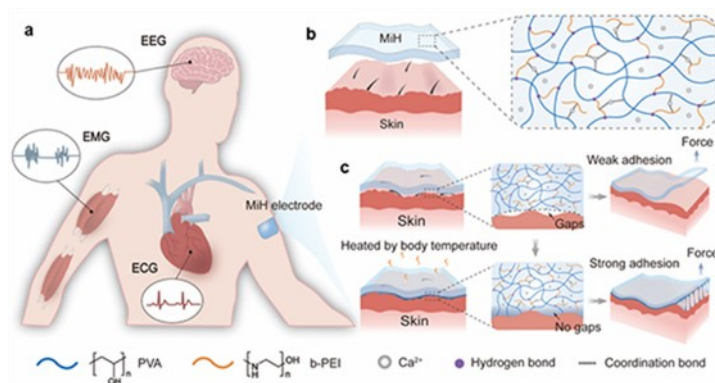
**Body temperature enhanced adhesive, antibacterial and  
recyclable ionic hydrogel for epidermal electrophysiological  
monitoring**

Ying Liu<sup>#</sup>, Chan Wang<sup>#</sup>, Jiangtao Xue<sup>#</sup>, Guanhua Huang,

Shuang Zheng, Ke Zhao, Jing Huang, Yiqian Wang, Yan Zhang,

Tailang Yin\*, Zhou Li\*

### ToC figure



The multifunctional ionic hydrogel (MiH) is equipped with body-temperature enhanced adhesion, stretchability, recyclability and antibacterial properties based on dual physical cross-linked network. When applied as the epidermal electrode, the MiH build a highly compliant and gapless interface with the skin, enabling the real-time monitoring of high-fidelity electrophysiological signals like EEG, ECG and EMG which brings intelligent functions and broaden the way for epidermal electronics, promotes the development of healthcare electronics.